



ELSEVIER

Available online at [www.sciencedirect.com](http://www.sciencedirect.com)

SCIENCE @ DIRECT®

Palaeogeography, Palaeoclimatology, Palaeoecology 217 (2005) 223–242

**PALAEO**

[www.elsevier.com/locate/palaeo](http://www.elsevier.com/locate/palaeo)

# Rising atmospheric CO<sub>2</sub> as a possible trigger for the end-Triassic mass extinction

Tran T. Huynh, Christopher J. Poulsen\*

*Department of Geological Sciences, University of Michigan, Ann Arbor, MI, USA*

Received 14 April 2004; received in revised form 15 November 2004; accepted 9 December 2004

## Abstract

The end-Triassic mass extinction, one of the five largest extinctions in Earth history, was a severe catastrophe in which 80% of all species were wiped out. The cause of the extinction is controversial, but any mechanism must account for mass extinction in both marine and terrestrial environments. One smoking gun—the eruption of the Central Atlantic Magmatic Province (CAMP)—has prompted the hypothesis that CO<sub>2</sub> degassing to the atmosphere may have induced an environmental catastrophe at the end-Triassic. In this study, we use a numerical coupled ocean–atmosphere climate model of the Late Triassic to determine environmental stresses associated with a rapid increase in atmospheric CO<sub>2</sub>. A series of sensitivity experiments, with CO<sub>2</sub> levels that bracket estimated end-Triassic *p*CO<sub>2</sub> estimates (2–8× pre-industrial levels), predict extreme environmental conditions. On land, increasing CO<sub>2</sub> from 2× to 8× pre-industrial levels causes an increase in the number and severity of hot days and days without precipitation, an exponential increase in continental area experiencing hot days, and enhanced seasonal fluctuation. In the ocean, wind-driven circulation decreases and meridional overturning diminishes by a factor of ~4, leading to enhanced ocean stratification. A three-box model of the deep ocean predicts a decline of ~85 μmol/L in deep ocean oxygen concentration with a 4-fold increase in atmospheric CO<sub>2</sub>. Consequently, while terrestrial organisms would have been subject to severe heat and water stress, marine fauna would have experienced oxygen deprivation. Additional sensitivity experiments indicate that variations in Milankovitch orbital parameters may further contribute to faunal stress by intensifying continental heating and seasonal fluctuations. In sum, model results predict that rising atmospheric CO<sub>2</sub> would have significantly impacted both marine and continental environments, providing a link between turnover on land and ocean during the Late Triassic.

© 2004 Elsevier B.V. All rights reserved.

*Keywords:* Paleoclimate; General circulation models; Triassic; Carbon dioxide; Mass extinction

## 1. Introduction

At the close of the Triassic, about 80% of all species went extinct (Sepkoski, 1996), and massive biotic turnover occurred in both the marine and terrestrial realms. Benton (1995) estimated that mean

\* Corresponding author. Tel.: +1 734 764 3362; fax: +1 734 763 4690.

*E-mail address:* [poulsen@umich.edu](mailto:poulsen@umich.edu) (C.J. Poulsen).

familial extinction rates were as high as 15.2–23.9% for all organisms, 10.6–23.4% for continental organisms, and 12.7–16.9% for marine organism. On land, almost half of all tetrapod species went extinct (Colbert, 1986), and more than 95% of megafloral species in Europe and North America disappeared (Visscher and Brugman, 1981; Fowell, 1994) while microfloral species exhibited significant turnover (Visscher and Brugman, 1981). The end-Triassic marine extinction, recognized as one of the “Big Five” events (Raup and Sepkoski, 1982), was also marked by the total collapse of the reef ecosystem (Hallam and Goodfellow, 1990) and extinctions among groups of cephalopods, bivalves, gastropods, and brachiopods (Hallam and Wignall, 1997). Microorganisms, including ostracods, foraminifera, coccolithophorids, radiolarians, and dinoflagellates, also underwent mass extinctions (El-Shaarawy, 1981; Bown and Lord, 1990).

Although evidence exists for catastrophic changes across the Triassic–Jurassic boundary, the “kill mechanism” for this extinction is still contested because environmental conditions associated with the T–J event are poorly known due the relative paucity of boundary sections worldwide (Hallam and Wignall, 1997). Various causes have been suggested for the mass extinction, including volcanism (Stothers, 1993; Courtillot, 1994; Marzoli et al., 1999; McElwain et al., 1999; Hesselbo et al., 2002), bolide impact (Olsen et al., 1987; Bice et al., 1992), sea level changes and anoxia (Hallam, 1981), and collapse in marine productivity (McRoberts and Newton, 1995). However, a feasible mechanism must explain the massive turnover rates observed both on land and at sea.

Linking the biotic turnover in the marine and terrestrial realms requires a “trigger” that can have global impact. Coincident timing of the end-Triassic event with the emplacement of the CAMP flood basalts (Hames et al., 2000; Pálffy et al., 2000; Hesselbo et al., 2002; Cohen and Coe, 2002) prompted the hypothesis that CO<sub>2</sub>-induced global warming, due to increased volcanism, caused the end-Triassic mass extinction (e.g., Stothers, 1993; Courtillot, 1994; Marzoli et al., 1999; McElwain et al., 1999). The CAMP eruptions reached peak intensity at 199.0±2.4 Ma (Marzoli et al., 1999; Hames et al., 2000). Age estimates of the mass extinction at the T–J boundary place the event close to 200 Ma (Pálffy et al.,

2000), with the terrestrial turnover preceding the marine extinction by ~600 ky (Pálffy et al., 2002). In addition to the consistent timing of the biotic crisis and CAMP eruptions at the T–J boundary, the postulated CO<sub>2</sub> increase likely had global ramifications and can potentially connect biotic events on the continents to those in the oceans.

Fossil stomatal characteristics (McElwain et al., 1999), geochemical proxies (Yapp and Poths, 1996; Suchecki et al., 1988; Ekart et al., 1999; Tanner et al., 2001; Beerling and Berner, 2002), and geochemical modeling (Berner and Kothavala, 2001; Beerling and Berner, 2002) provide a means of estimating the magnitude of CO<sub>2</sub> increase across the T–J boundary. Although the lowest *p*CO<sub>2</sub> level suggested for the Late Triassic is approximately 600 ppmv (McElwain et al., 1999), the majority of estimates are around 1500 ppmv and compilations of all available *p*CO<sub>2</sub> estimates suggest that on average *p*CO<sub>2</sub> increased by 2- to 3-fold across the T–J boundary (Royer et al., 2001; Beerling and Berner, 2002). The range of estimated CO<sub>2</sub> rise are from a moderate increase of ~250 ppmv (Tanner et al., 2001) to a 4-fold increase (McElwain et al., 1999) from Late Triassic levels. However, the relative stability suggested by Tanner et al. (2001) has been contested on the basis that the temporal resolution of the paleosol samples may have been inadequate to detect a rapid, transient rise in atmospheric CO<sub>2</sub> (Beerling and Berner, 2002; Retallack, 2002), and that the carbon isotopic composition of terrestrial organic matter within the paleosol was not considered. After re-calibrating the paleo-barometer to account for the natural isotopic variations in terrestrial organic matter, Beerling and Berner (2002) estimated a CO<sub>2</sub> rise of 1032 ppmv. Based on biogeochemical modeling of the T–J carbon cycle perturbation, Beerling and Berner (2002) suggested that CO<sub>2</sub> degassing alone could not fully account for the substantial negative carbon isotopic excursion (up to -3.5‰) recorded in marine carbonate, organic matter, and terrestrial wood (McElwain et al., 1999; Ward et al., 2001; Pálffy et al., 2001; Hesselbo et al., 2002). Instead, they suggest that degassing of volcanogenic CO<sub>2</sub> triggered the release of massive amounts of CH<sub>4</sub> into the ocean–atmosphere system by destabilizing methane hydrate reservoirs. The rapid oxidation of CH<sub>4</sub> to CO<sub>2</sub> would have the net effect of raising atmospheric *p*CO<sub>2</sub> to values in excess of 2500

ppmv by Early Jurassic times (Beerling and Berner, 2002).

Given the likely rise in atmospheric  $p\text{CO}_2$  at the T–J boundary, the aim of this paper is to test the hypothesis that rising atmospheric  $\text{CO}_2$  triggered the end-Triassic mass extinction. To this end, a series of Late Triassic  $\text{CO}_2$  sensitivity experiments have been conducted using a fully coupled ocean–atmosphere general circulation model. Using these experiments, we evaluate possible linkages between atmospheric  $p\text{CO}_2$  increase and biotic turnover by (1) assessing which components of the Late Triassic climate system are sensitive to atmospheric  $\text{CO}_2$  rise, (2) identifying potential biotic stresses resulting from an increase in  $\text{CO}_2$  levels, and (3) evaluating the magnitude of  $p\text{CO}_2$  change required to drive biotic turnover.

## 2. Model description and experiments

The Late Triassic climate experiments were completed using the Fast Ocean Atmosphere Model (FOAM) version 1.5, a fully coupled mixed-resolution ocean and atmosphere GCM. The atmospheric model is a parallelized version of the Community Climate Model 2 (CCM2) with the radiative and hydrological physics upgraded to the equivalent of CCM3 version 3.2 (Kiehl et al., 1996). The atmospheric component of FOAM was run at spectral resolution R15 ( $4.5^\circ \times 7.5^\circ$ ) with 18 vertical levels. The ocean component of FOAM (OM3) is a  $z$ -coordinate ocean general circulation model developed following the GFDL MOM model with a  $128 \times 128$  point Mercator grid ( $1.4^\circ \times 2.8^\circ$ ) and 16 vertical levels. The land surface model in FOAM divides the land surface into five main vegetation types, according to Matthews' classification scheme (Matthews, 1983). A four-layer diffusion model calculates temperatures using the thermal properties and thickness of the vegetation type. Furthermore, the land surface model uses a simple bucket model with a 15 cm deep bucket and evaporation is a function of the water depth of the bucket. The various components of the model are linked through a coupler, which was designed to accommodate the differing ocean and atmosphere model resolutions. A more detailed description of FOAM components is available in Jacob et al. (2001) and Jacob (1997).

FOAM has been widely used to study climate change through geologic time (e.g., Liu et al., 2000; Poulsen, 2001; Wu and Liu, 2002; Harrison et al., 2003; Poulsen et al., 2003; Pierrehumbert, 2004). FOAM's simulation of modern climate shows reasonable agreement with present-day observations. In addition to the mean climate state, FOAM successfully simulates many aspects of modern interannual and interdecadal variability (Jacob, 1997; Liu et al., 2000). FOAM's most important shortcoming is an underestimation of North Atlantic Deep Water production, a problem common to coupled ocean–atmosphere models. Considering the tremendous differences between modern and Late Triassic continental positions (i.e., the Atlantic Ocean did not exist in the Triassic), we do not consider this to be a significant limitation on our ability to model Late Triassic climate. In a recent comparison of the simulation of global upper ocean circulation between FOAM and the NCAR Community Climate System Model (CCSM), Liu et al. (2003) showed that in many regions the two models respond consistently to Holocene orbital forcing. In fact, FOAM's sensitivity to a doubling of atmospheric  $p\text{CO}_2$  is similar to that of the CCSM (Dr. Robert Jacob, personal communication, 2004), approximately  $2^\circ\text{C}$  or  $0.5\text{ C/W/m}^2$  and roughly a factor of 2 lower than NOAA's GFDL model and UKMO's Hadley Center model (CCSM Science Plan, 2003).

To test the effect of atmospheric  $p\text{CO}_2$  forcing on the Triassic climate system, a series of  $\text{CO}_2$  sensitivity experiments were conducted with two, four, six, and eight times (hereafter referred to as 2–8 $\times$ ) the pre-industrial level of 300 ppmv (after Berner and Kothavala, 2001). All other boundary and initial conditions remain constant between experiments. The 2–8 $\times$  scenarios encompass the 4-fold increase in atmospheric  $\text{CO}_2$  across the T–J boundary suggested by McElwain et al. (1999). Most other estimates of Late Triassic  $p\text{CO}_2$  indicate that minimum levels were approximately four times pre-industrial levels. On the other hand, biogeochemical modeling and paleosol analyses suggest maximum atmospheric  $p\text{CO}_2$  levels may have been greater than 2500 ppmv. Our choice of atmospheric  $p\text{CO}_2$  values falls within the estimated range of  $p\text{CO}_2$ , but should probably be considered to be a conservative estimate of the total possible rise in  $p\text{CO}_2$  at the end-Triassic.

The Triassic experiments were designed with the Late Triassic paleogeography and paleotopography of Scotese et al. (1994). Due to the lack of preserved seafloor of Triassic age, ocean depths beyond the continental shelf were set to 4800 m. The model solar luminosity was reduced to 98% of the present-day level ( $1367 \text{ Wm}^{-2}$ ) to account for increasing fusion rate in the solar core with time (Endel and Sofia, 1981). Other atmospheric gas trace gas concentrations, including  $\text{CH}_4$ ,  $\text{N}_2\text{O}$ , and ozone, were set to pre-industrial levels. In the initial suite of simulations, model eccentricity, obliquity, precession, and rotation rate were set to present-day values. Because EBM calculations have shown that Pangean surface temperatures could vary as much  $16^\circ\text{C}$  with reasonable changes in orbital parameters (Crowley and Baum, 1992), two additional experiments were run to assess how orbital parameters might have contributed to Late Triassic climatic stresses. Two different orbital configurations for the  $8\times$  simulation were tested to determine the range of climate conditions possible under scenarios of maximum summer insolation in the Southern and Northern Hemispheres (*shsm* and *nshsm*, respectively). In both cases, an eccentricity of 0.06 and an obliquity of  $24.5^\circ$  were used, and the summer solstice of the respective hemisphere occurs at perihelion.

Uniform land surface characteristics were specified in all experiments. Each land grid cell was given the surface characteristic of a deciduous forest—the mean vegetation type in the Matthews (1983) classification scheme. A number of factors drove the decision to use simplified land surface characteristics. The most important factor was the absence of paleo-vegetation reconstructions that bracket the end-Triassic event. Because land surface characteristics—and particularly regional differences in surface characteristics—can influence atmospheric dynamics (such as the subsiding branch of the Hadley circulation), we chose not to include these details. Our concern is that without detailed knowledge of the evolution of paleo-vegetation through the end-Triassic, we would be introducing a factor that will significantly alter the climate's

response to a rise in  $p\text{CO}_2$ . While this decision to use uniform vegetation characteristics might not lead to the optimal simulation of the Late Triassic climate, it is essential for producing robust sensitivity experiments. In the future, we hope to incorporate a dynamic biome model that will explicitly treat climate–vegetation interactions.

The Triassic  $2\text{--}8\times$  experiments were integrated for 600 years without flux corrections or deep ocean acceleration. The ocean model was run using a fixed diffusion coefficient. During the last 100 years of model integration, there is no apparent drift in the upper ocean (between the surface and 300 m depth), and  $<0.0007^\circ\text{C}/\text{year}$  change in globally averaged ocean temperature.

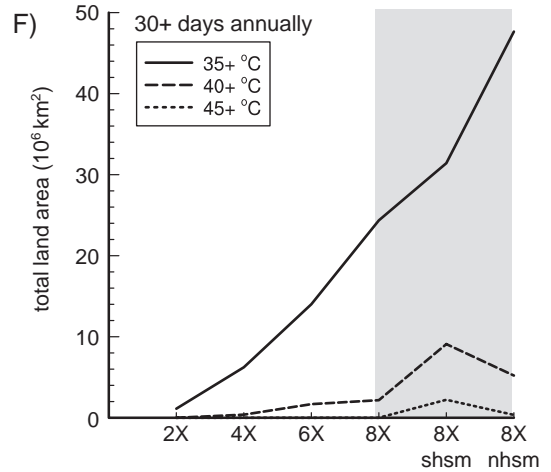
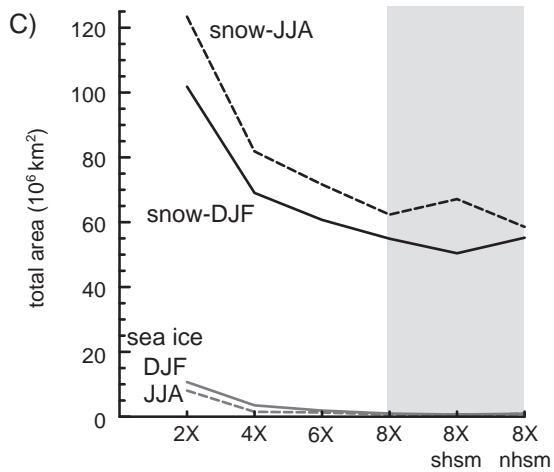
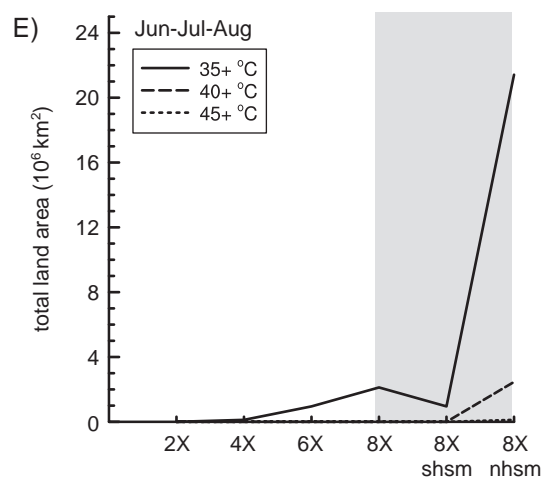
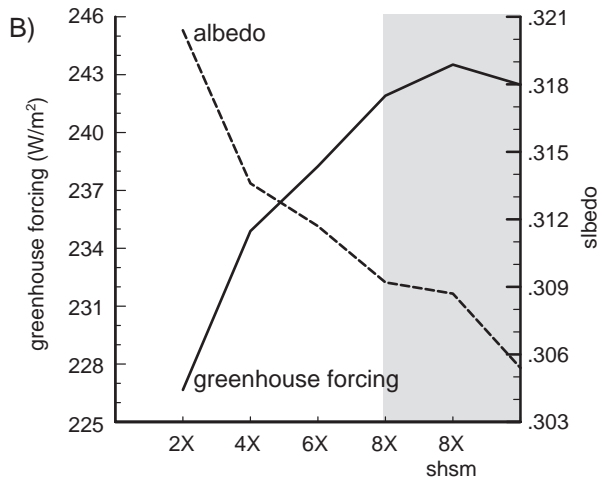
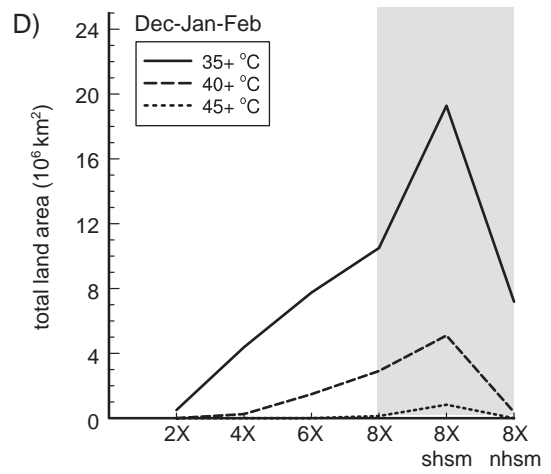
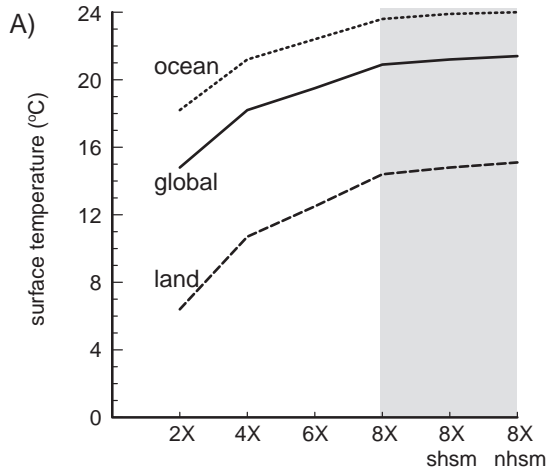
The Late Triassic experiments represent equilibrium climate states at particular levels of atmospheric  $p\text{CO}_2$  and should thus be viewed as end-member climate states (before and after the in  $p\text{CO}_2$ ). Without the ability to run FOAM for hundreds of thousands of years, it is impossible to fully mimic the transient  $\text{CO}_2$  rise of the end-Triassic. The results shown here are derived from monthly averages of the last 25 years of the model integration. Because monthly averaging filters out climate extremes that may represent significant stresses on organisms, daily average values of the physical fields were also computed for the last 3 years of model integration.

### 3. Results

#### 3.1. $\text{CO}_2$ sensitivity on land

Globally warm temperatures, extreme seasonality, and high aridity characterize Pangean climate in the Late Triassic simulations. Temperatures are predicted to increase at greater amounts of atmospheric  $\text{CO}_2$ , with the largest magnitude occurring on land due to its lower specific heat relative to the ocean (Fig. 1A). Increasing  $p\text{CO}_2$  from  $2\times$  to  $8\times$  pre-industrial levels raises the average surface–air temperature by  $6.1^\circ\text{C}$

Fig. 1. Globally averaged mean annual (A) surface temperatures in  $^\circ\text{C}$ ; (B) greenhouse forcing and albedo in  $\text{W}/\text{m}^2$ ; (C) total area covered in seasonal sea ice and snow in  $10^6 \text{ km}^2$ ; (D) total area in excess  $35$ ,  $40$ , and  $45^\circ\text{C}$   $10^6 \text{ km}^2$  during austral summer; (E) total area in excess  $35$ ,  $40$ , and  $45^\circ\text{C}$   $10^6 \text{ km}^2$  during boreal summer; and (F) total area with more than 30 consecutive days in excess  $35$ ,  $40$ , and  $45^\circ\text{C}$  in  $10^6 \text{ km}^2$  for all experiments. Model results indicate that increasing atmospheric  $\text{CO}_2$  substantially increases extreme climatic conditions on land.



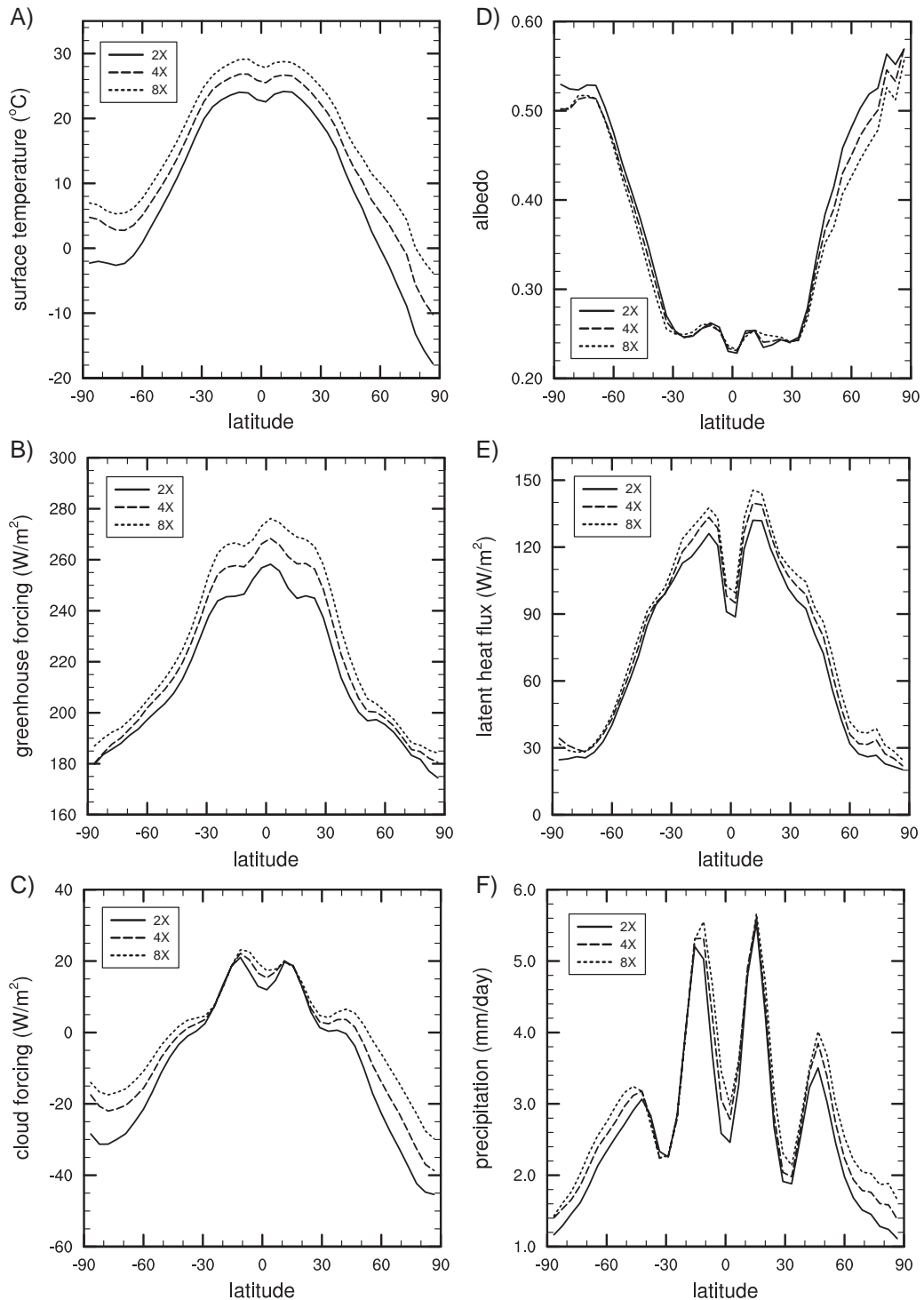


Fig. 2. Zonally averaged (A) surface temperatures in  $^{\circ}\text{C}$ ; (B) greenhouse forcing in  $\text{W/m}^2$ ; (C) cloud forcing in  $\text{W/m}^2$ ; (D) albedo; (E) latent heat flux  $\text{W/m}^2$ ; and (F) sensible heat flux in  $\text{W/m}^2$  for 2 $\times$  (solid line), 4 $\times$  (long dashed line), and 8 $\times$  (short dashed line) experiments.

globally and 8.0 °C on land, compared to 5.4 °C over the oceans. The increased temperatures in scenarios with higher  $p\text{CO}_2$  are due primarily to an enhanced greenhouse effect (Figs. 1B and 2B) resulting from greater atmospheric water vapor, as evidenced by the greater surface latent heat flux (Fig. 2E), and an increase the amount of solar radiation reaching the surface reduction due to a reduction in low and medium cloud cover (Fig. 2C). The greenhouse forcing is most effective in the tropics (Fig. 2B), whereas at high latitudes—where the magnitude of surface temperature rise is the greatest—higher temperatures result from a decrease in surface albedo due to a

reduction in snow and sea ice extent (Figs. 1C and 2D) and an increase in the cloud forcing (Fig. 2C). The warmer continental temperatures further reduce the seasonal snow cover (Fig. 1C), which acts as a positive feedback to global warming.

In all Triassic simulations, the warmest temperatures occur in the vast subtropical interior lowlands of the Southern Hemisphere (Figs. 3A–C and 4). The average summer temperature in this area for the 2×, 4×, and 8× experiment is ~32, 36, and 42 °C, respectively. Maximum summer temperatures are typically 4–8 °C higher than the seasonal average (Fig. 4). In the Northern Hemisphere, subtropical

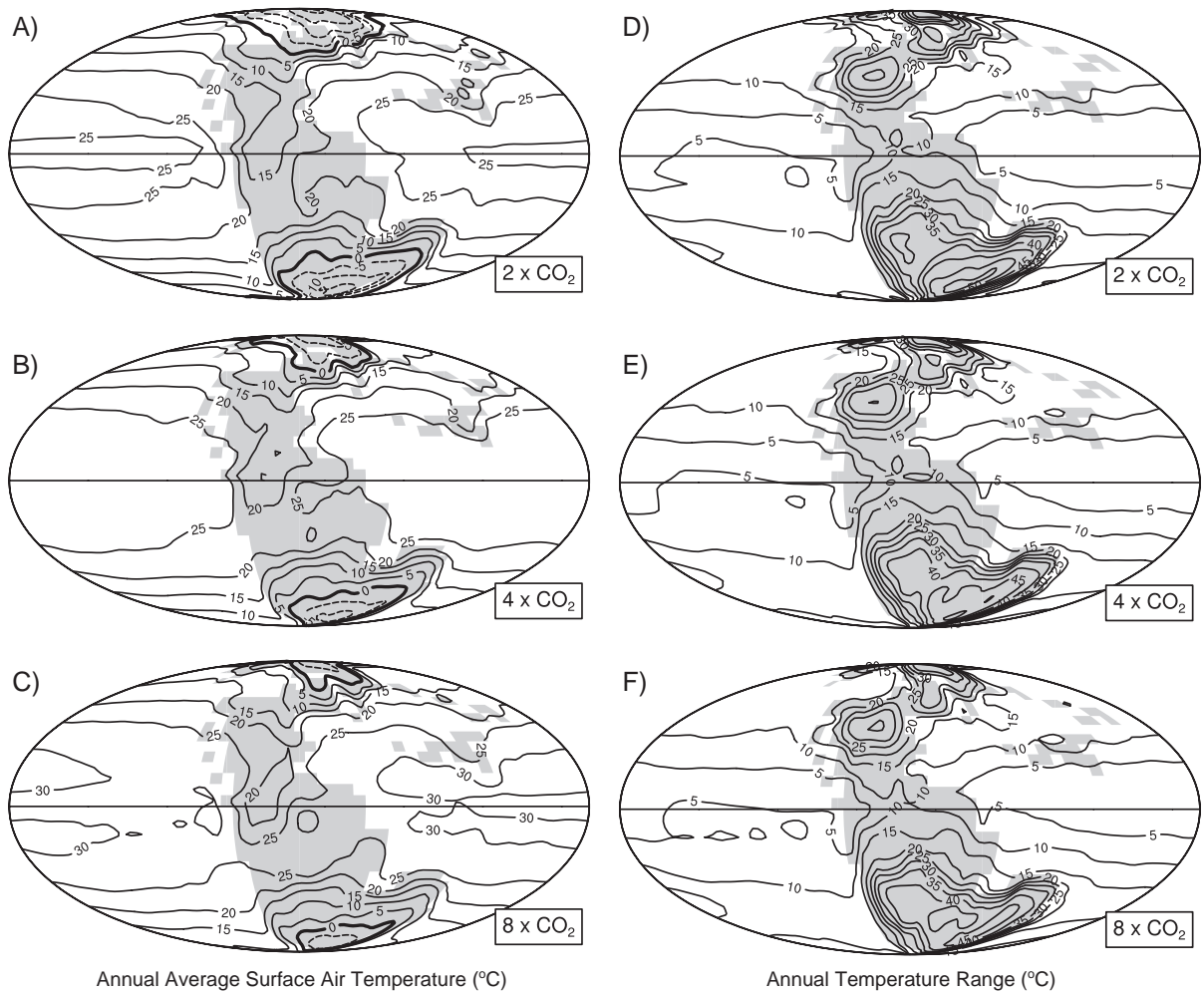


Fig. 3. Annual average surface temperatures (left panel, A–C) and temperature range in °C (right panel, D–E) 2×, 4×, and 8× experiments. Land area is shaded in gray. With an increase from 2× to 8×  $p\text{CO}_2$ , mean annual temperatures increase by >5 °C over much of Pangea. In all experiments, high and mid-latitudes experience tremendous seasonal temperature fluctuations.

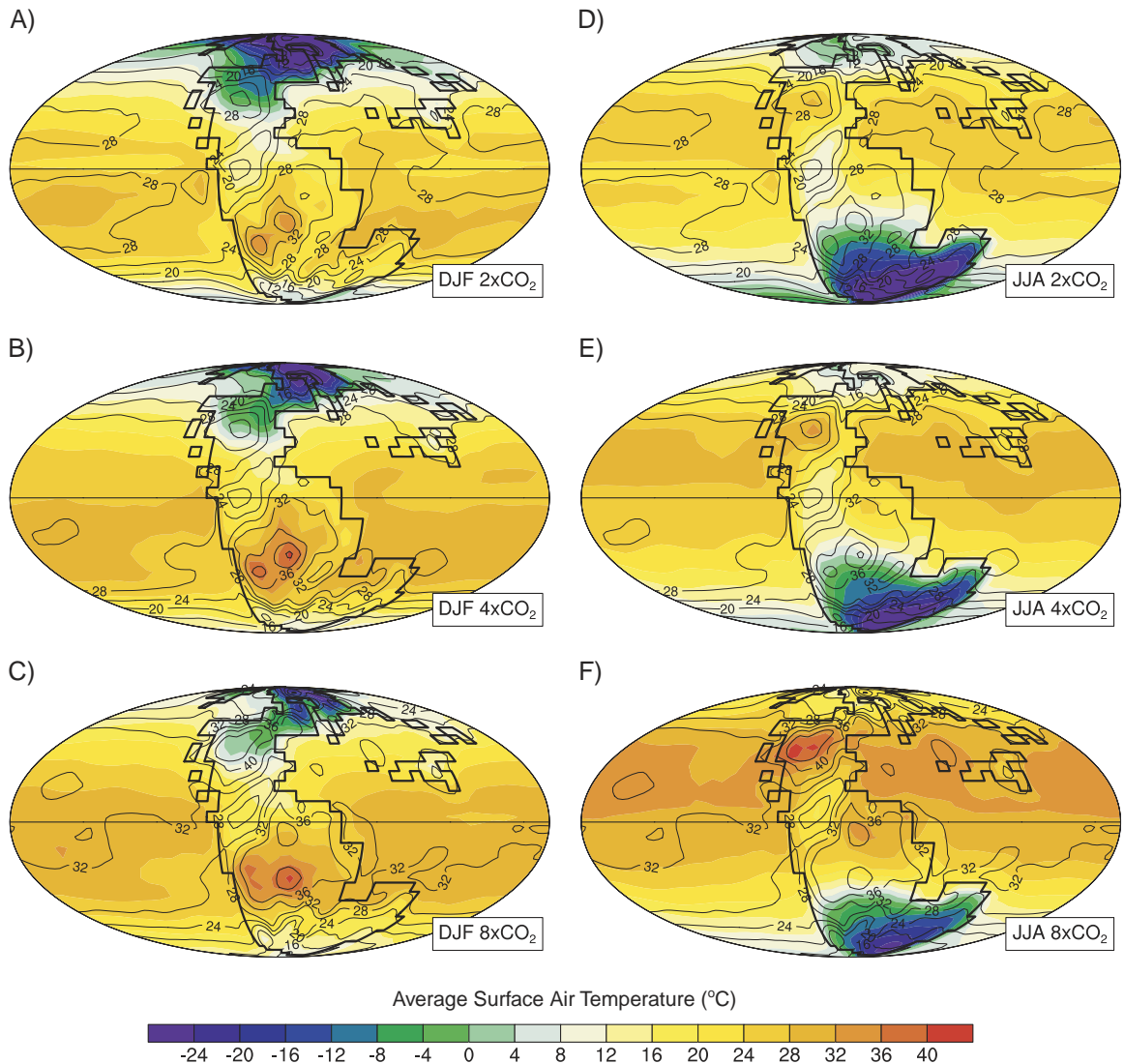


Fig. 4. Summer and winter average air surface temperature (color), overlain by maximum annual temperature annually (contour lines) for the 2× and 8× simulations (years 598–600). Note that DJF and JJA figures are overlain with the same maximum temperature contours. The contour interval of 4 °C. Land area is outlined in bold black. Model results indicate that seasonal and maximum temperatures increase significantly with higher atmospheric  $p\text{CO}_2$ . For example, in subtropical regions, maximum temperatures increase by 4–12 °C between the 2× and 8× experiments causing them to rise well above 35 °C in some regions.

surface temperatures are not as severe as in the south. Boreal summer temperatures are ~28, 32, and 36 °C on average with maximum temperatures approximately +4 °C of that value for the 2×, 4×, and 8× simulations, respectively (Fig. 4A–C).

Extreme seasonal temperature fluctuations are also characteristic of Pangea during the Late Triassic. Along with the poleward expansion of warmer areas

during the summer season, cold areas are more restricted during the winter when atmospheric CO<sub>2</sub> increases (Figs. 3A–C and 4). Nevertheless, the annual continental temperature range simulated for the Late Triassic is still much greater than that observed on the modern-day Eurasian landmass. The annual temperature range in the southern high latitudes is +55 °C, and +40 °C in the Northern

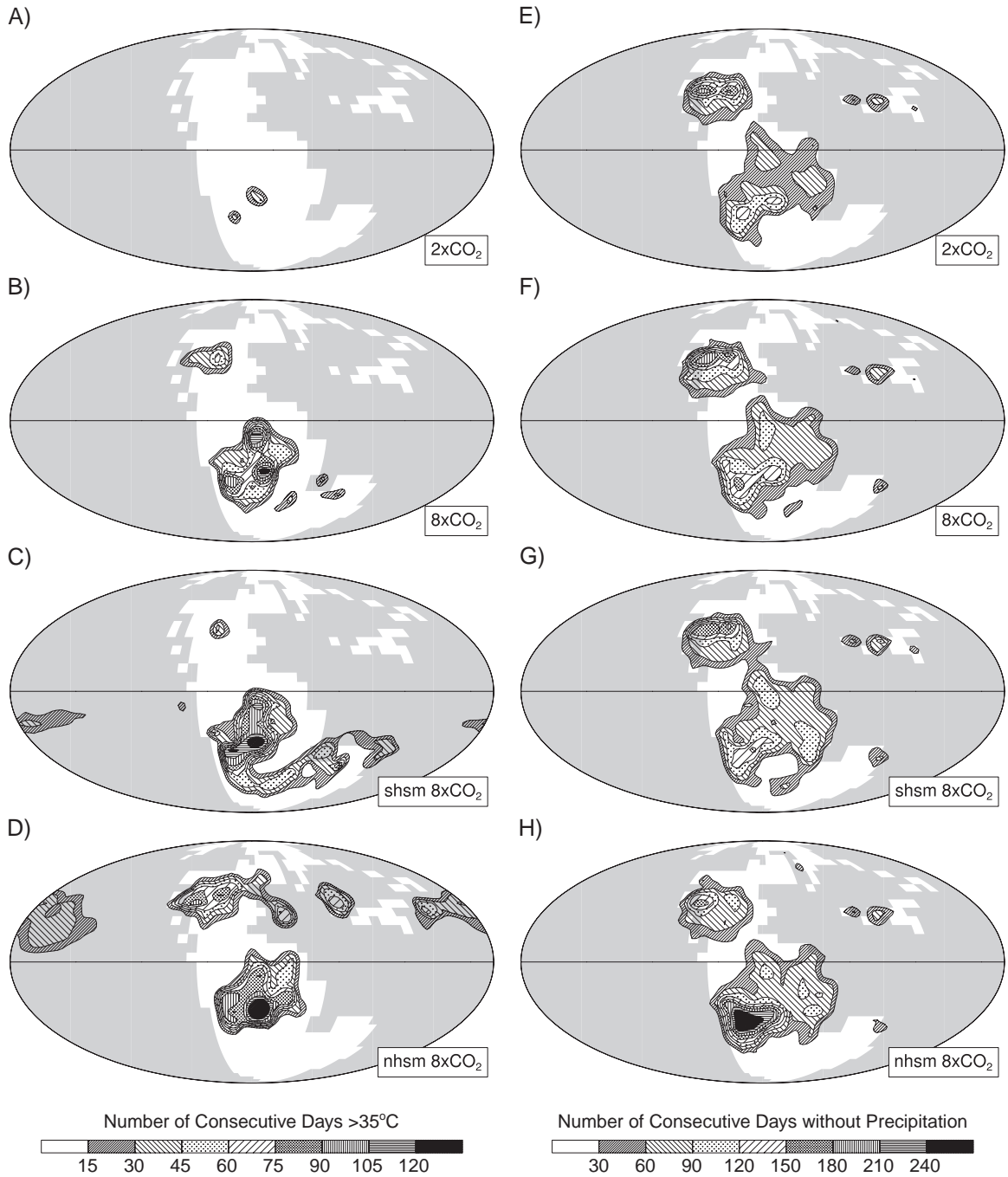


Fig. 5. Total number of consecutive days per year where temperatures exceeded 35 °C (left panel, A–D) and consecutive days without precipitation (right panel, E–H) in 2× and 8× simulations (years 598–600). Also shown are the results from orbital variations in which insolation was set maximum summer insolation values for the Northern (*nhsm*) and Southern (*shsm*) Hemispheres. Land area is shaded white. Late Triassic model results demonstrate that changes in atmospheric  $p\text{CO}_2$  and orbital parameters can significantly enhance extreme climatic conditions on Pangea.

Hemisphere at low  $p\text{CO}_2$  levels. Only in central Siberia, Mongolia, and central Canada are such extreme ranges approached today. In the tropics (0–20° latitude) and mid-latitudes (30–50° latitude), the simulated temperature ranges are as high as 10–20 °C and 20–30 °C, respectively, somewhat larger than modern ranges.

Continental warming at higher  $p\text{CO}_2$  levels is accompanied by both an expansion in land area affected by hot temperatures and aridity, as well as an increase in the number of high temperature days (Figs. 1D–F and 5A–B). For example, when  $\text{CO}_2$  is raised from 2× to 8×, the total land surface area in

excess of 35 °C during the austral summer increases by 20-fold (Fig. 1D; Table 1B). While no continental areas in the 2× simulation exceed 40 °C, the 8× scenario has ~2.91 million  $\text{km}^2$  where temperatures rise above 40 °C during the austral summer (Fig. 1D; Table 1B). Another consequence of elevated atmospheric  $\text{CO}_2$  is an increase in the number of very hot days (Table 1B; Fig. 5A–B). The total land area with >35 °C temperatures for more than 30 consecutive days increases by at least 20-fold between 2× and 8× experiments (Table 1B; Fig. 5A–B). In the 2× simulation, the hottest areas experience up to 40 consecutive days of temperatures >35 °C (Fig. 5A).

Table 1

(A) Mean annual surface–air temperatures and areal extent of seasonal sea ice and snow cover. (B) Total land surface area ( $10^6 \text{ km}^2$ ) affected by hot temperatures. (C) Mean annual ocean temperatures, total upwelling volume (Sv), and calculated dissolved oxygen concentration ( $\mu\text{mol/L}$ )

(A) Results averaged from years 576–600

Experiment	Surface–air temperature (°C)			Total surface area ( $10^6 \text{ km}^2$ )			
	Global	Land	Ocean	DJF sea ice	JJA sea ice	DJF snow	JJA snow
2× $\text{CO}_2$	14.8	6.4	18.2	10.67	8.05	101.80	123.42
4× $\text{CO}_2$	18.2	10.7	21.2	3.50	1.50	69.03	81.84
6× $\text{CO}_2$	19.5	12.5	22.4	1.87	1.29	60.71	71.64
8× $\text{CO}_2$	20.9	14.4	23.6	0.95	0.64	54.91	62.35
<i>shsm</i> 8× $\text{CO}_2$	21.2	14.8	23.9	0.64	0.52	50.41	67.13
<i>nhs</i> m 8× $\text{CO}_2$	21.4	15.1	24.0	0.92	0.82	55.21	58.56

(B) Total land surface area affected ( $10^6 \text{ km}^2$ )

Experiment	Dec.–Jan.–Feb.			Jun.–Jul.–Aug.			30+ days annually		
	>35 °C	>40 °C	>45 °C	>35 °C	>40 °C	>45 °C	>35 °C	>40 °C	>45 °C
2× $\text{CO}_2$	0.50	–	–	–	–	–	1.12	–	–
4× $\text{CO}_2$	4.38	0.25	–	0.12	–	–	6.23	0.38	–
6× $\text{CO}_2$	7.75	1.48	–	0.95	–	–	14.01	1.68	–
8× $\text{CO}_2$	10.50	2.91	0.13	2.12	–	–	24.36	2.17	–
<i>shsm</i> 8× $\text{CO}_2$	19.28	5.10	0.83	0.95	–	–	31.42	9.09	2.22
<i>nhs</i> m 8× $\text{CO}_2$	7.19	0.37	0.00	21.42	2.46	0.12	47.66	5.21	0.35

(C) Ocean results averaged from years 576–600

Experiment	Ocean temperature (°C)				Upwelling (Sv)		[O <sub>2</sub> ] ( $\mu\text{mol/L}$ )
	Global	10 m	50 m	100 m	DJF	JJA	Surface ocean
2× $\text{CO}_2$	1.8	14.6	10.9	10.1	25.66	46.72	320
4× $\text{CO}_2$	4.7	17.6	13.5	12.7	22.64	43.03	301
6× $\text{CO}_2$	5.1	18.7	14.5	13.6	22.61	41.12	294
8× $\text{CO}_2$	6.8	20.0	15.8	14.6	21.26	39.38	287
<i>shsm</i> 8× $\text{CO}_2$	6.8	20.4	15.9	14.9	20.25	38.09	284
<i>nhs</i> m 8× $\text{CO}_2$	7.1	20.4	15.9	14.9	21.15	41.24	284

Upwelling is defined where the mean upper ocean (<200 m) vertical velocity is negative (upward). Because the vertical diffusion coefficient is constant, only the advective flux is estimated. Dissolved O<sub>2</sub> content was calculated from predicted surface ocean temperatures and salinity, based on relationship established by Weiss (1970). All results were averaged for the last 25 model integration years (years 576–600).

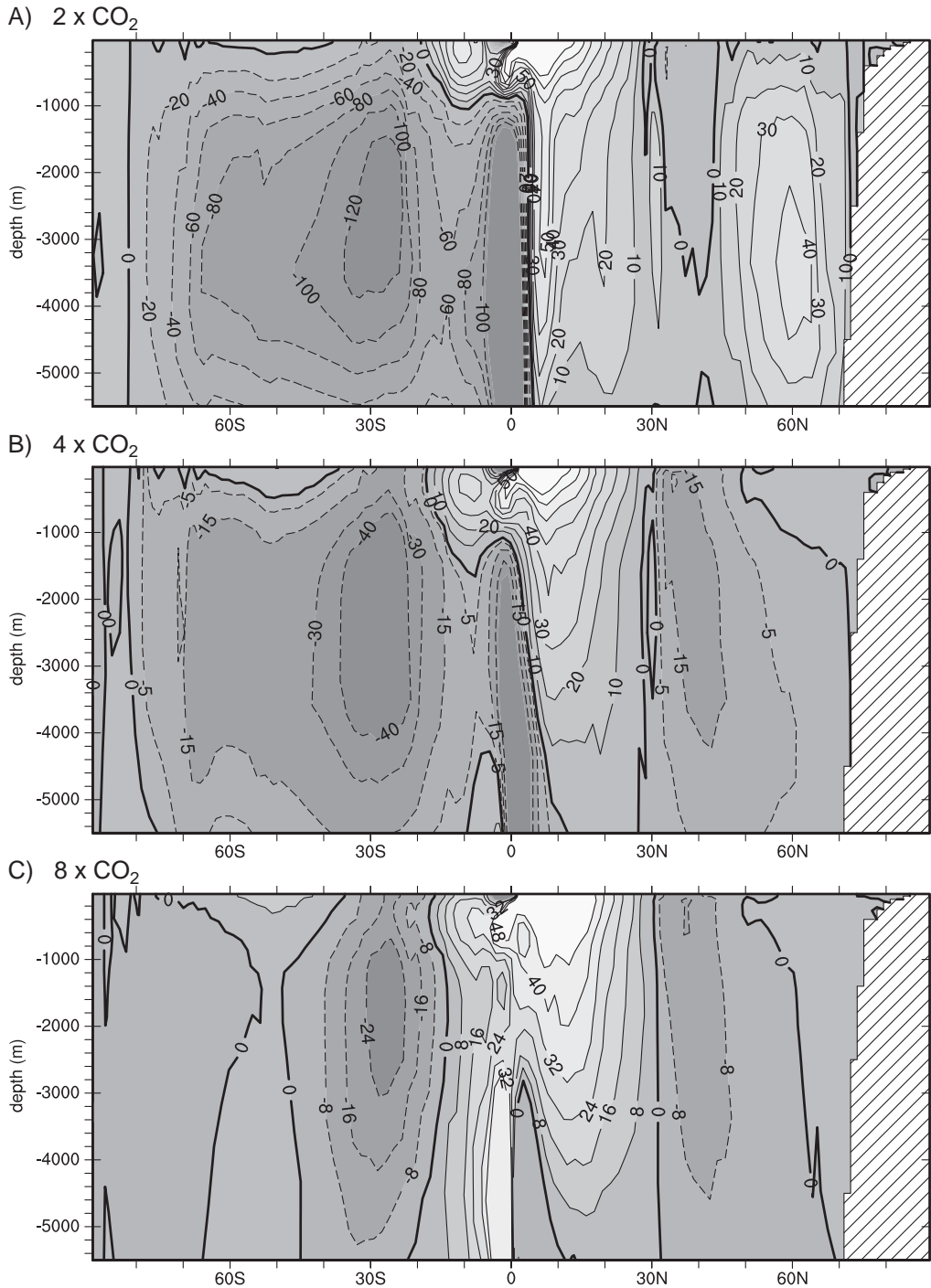


Fig. 6. Meridional oceanic overturning, measured in Sverdrups [ $10^6 \text{ m}^3/\text{s}$ ] for 2 $\times$ , 4 $\times$ , and 8 $\times$  experiments. Positive values (solid lines) indicate counterclockwise flow, and negative values (dashed lines) indicate flow in the clockwise direction. Contour lines are labeled unevenly for better visualization. Meridional overturning is substantially reduced with increased atmospheric CO<sub>2</sub> levels. At high latitudes, the overturning circulation nearly disappears in the 8 $\times$  experiment.

Increasing  $p\text{CO}_2$  to 2400 ppmv results in the lowland areas of southern Pangea experiencing ~110 consecutive days with temperatures  $>35^\circ\text{C}$  (Fig. 5B), during which ~60 days have temperatures  $>40^\circ\text{C}$ . Accompanying the extremely hot days are more than 135 and 200 consecutive days without any precipitation in the Southern and Northern Hemispheres, respectively, for 2–8 $\times$  simulations (Fig. 5E–F). In the subtropics, these simulated climate conditions are comparable to what is observed in the modern Sahara desert during extremely dry, hot years.

### 3.2. $\text{CO}_2$ sensitivity in the oceans

In the elevated  $\text{CO}_2$  experiments, enhanced surface radiation receipt also produces significantly warmer ocean temperatures, but the increases are not as great as on land due to the higher heat capacity of the ocean (Fig. 1A). In fact, the seasonal seawater temperature fluctuations in ocean temperatures in all Triassic simulations are within the modern observed range ( $<10^\circ\text{C}$ ). Globally averaged mean annual ocean temperatures rise by  $5^\circ\text{C}$  with a 5-fold  $p\text{CO}_2$  increase from 600 to 2400 ppmv (Table 1C). The greatest warming occurs in the surface ocean: temperatures increase by  $5.4^\circ\text{C}$  at 10 m depth,  $4.9^\circ\text{C}$  at 50m, and  $4.5^\circ\text{C}$  at 100 m (Table 1C).

The increase in atmospheric  $p\text{CO}_2$  leads to a substantial reduction in surface and deep ocean circulation. In response to higher  $p\text{CO}_2$ , the hydrological cycle intensifies, leading to increased precipitation (by approximately 20–25% at  $60^\circ$ ; Fig. 2F) and runoff rates at high latitudes. Higher freshwater forcing combined with the warmer ocean temperatures reduces the low- to high-latitude density gradients and acts to inhibit meridional overturning and convective mixing. Meridional oceanic overturning diminishes at least 4-fold (from 60+ to 10–20 Sverdrups) in the southern extratropical ocean between the 2 $\times$  and 8 $\times$  experiments (Fig. 6). At high latitudes, the overturning circulation nearly disappears in the high latitudes of the 8 $\times$  experiment (Fig. 6C). In addition, convective mixing at high latitudes is reduced by  $>50\%$  between the 2 $\times$  and 8 $\times$  experiments; both the frequency and area of convective mixing is diminished in the 8 $\times$  experiment (not shown). Wind-driven surface ocean circulation also decreases at elevated  $p\text{CO}_2$  levels, as indicated

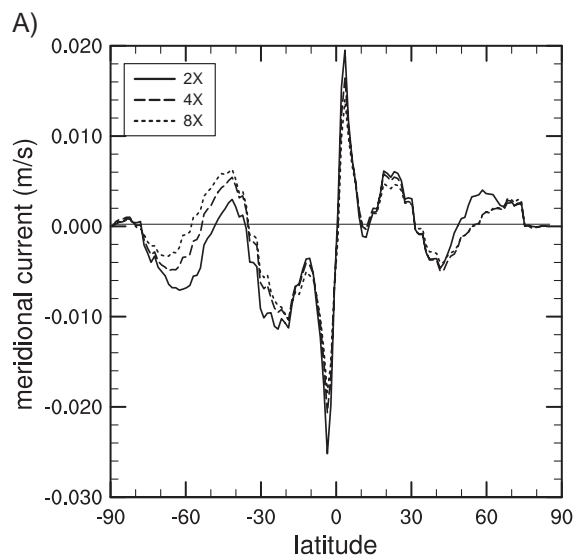


Fig. 7. (A) Meridional surface ocean current [m/s], average over the top 100 m. Positive (negative) numbers indicate northward (southward) flow direction.

by a reduction in zonally averaged meridional velocity in the upper ocean (Fig. 7B). Consequently, the volume of water upwelled to the surface ocean is also diminished. The Triassic experiments predict that a 4-fold increase in  $p\text{CO}_2$  reduces the total volume of water upwelled by 16–17% (Table 1C). In sum, in the Triassic simulations, the ocean's responses to increasing atmospheric  $\text{CO}_2$  levels include global ocean warming, enhanced upper-ocean stratification, and reduction of both surface and deep ocean circulation.

### 3.3. Effect of orbital configuration

The Late Triassic Pangean continental surface temperatures are highly sensitive to orbital forcing, as first noted by Crowley and Baum (1992). The simulations demonstrate that changes in orbital configurations, by altering the patterns of solar insolation received, can further intensify the simulated climatic extremes on land. Global mean annual average surface temperatures are  $0.3$ – $0.7^\circ\text{C}$  greater in the *nhs*m and *shsm* simulations than in the 8 $\times$  experiment with modern orbital settings (Fig. 1A; Table 1A). Summer temperatures are especially sensitive to orbital forcing. In the Southern Hemisphere, *nhs*m configuration

reduces average and maximum temperatures 4–8 °C, while *shsm* configuration raises temperatures ~4 °C. In the Northern Hemisphere, subtropical surface temperatures are not as severe as in the Southern Hemisphere, but still reach extremely high values with an *nhs*m orbital configuration. In addition, orbital variations influence the total land area affected by, as well as the duration of, such extreme conditions on land. In comparison to the 8× experiment, total land surface area in excess of 35 °C during austral summer increases by ~50% in the *shsm* experiment, but decreases ~30% in the *nhs*m case (Table 1B; Figs. 1D and 5B–D). The 8× experiment predicts an area of ~2.91 million km<sup>2</sup> with temperatures greater than 40 °C during the austral summer; the *shsm* orbital configuration leads to a 2-fold increase (Table 1B; Fig. 1D). In the Northern Hemisphere, summer temperatures on land never surpass 40 °C under modern orbital settings, but ~2.46 million km<sup>2</sup> are predicted to experience temperatures >40 °C with an *nhs*m configuration (Table 1B; Fig. 1E). Under maximum summer insolation, the total land area with >35 °C temperatures for more than 30 consecutive days increases by 50–100% (Table 1B; Figs. 1F and 5B–D). Orbital forcing, however, does not appear to significantly impact ocean temperatures, although insolation variations influence the volume of seasonally upwelled seawater (Table 1C).

### 3.4. Potential terrestrial biotic stresses

In modern organisms, rising temperatures cause a number of physiological changes, including increased oxygen demand due to an increase in their metabolic rate (cf. Pörtner, 2001); an exponential rise in the cell membrane permeability, requiring massive inputs of energy to compensate for the dissipative ion movements (Moseley et al., 1994); higher production of oxygen radicals linked to oxidative stress (Rifkind et al., 1993); and eventual collapse of ventilatory and circulatory functions due to progressive hypoxia in the body fluids in cases of prolonged heat stress (Pörtner, 2002). These physiological changes lead to the disruption of growth and reproduction in individual organisms, and will adversely affect the population dynamics in a matter of weeks to months (Pörtner, 2002). The climate thresholds that trigger physiological changes in modern organism are species-specific

(Walther et al., 2002); whether these thresholds differed in Triassic organisms is unknown. Biogeographic studies have shown that climate exerts a dominant control over the distribution of species in the modern day, as well as in the past (e.g., Walther et al., 2002; Woodward, 1987; Huntley, 1999; Davis and Shaw, 2001). Thus, any significant changes in environmental parameters are expected to impact biodiversity patterns in the past. The Triassic simulations predict that rising atmospheric CO<sub>2</sub> will lead to ubiquitous warming, with the greatest warming occurring on land. In fact, the results suggest that increasing atmospheric CO<sub>2</sub> will lead to (1) extreme continental heating, (2) intense seasonal fluctuations of surface temperatures, (3) an increase in the number of hot days and days without precipitation, and (4) an exponential rise in the land surface area affected by heat and aridity (Section 3.1). These climatic responses to elevated atmospheric CO<sub>2</sub> represent potential stresses on terrestrial organisms, and ecosystems.

### 3.5. Potential marine biotic stresses

In response to a rise in atmospheric CO<sub>2</sub>, the marine biota, on the other hand, must contend with a different set of environmental stresses arising from diminished surface and deep ocean circulation. The resulting ocean stratification will adversely affect marine life by lowering the oxygen availability in the water column. To quantify the potential decrease in oxygen availability, we have constructed a simple open-system, three-box model of the ocean, following the example of Hotinski et al. (1999). The box model predicts the oxygen concentration in three ocean reservoirs (shallow low-latitude, shallow high-latitude, and deep ocean reservoirs) as a function of biological productivity, which is linked directly to nutrient concentration (phosphate) through the Redfield ratio. A schematic of the box model, the governing equations, and model parameters are shown in Fig. 8 and Table 2. Note that all of our box-model sensitivity experiments were run from a modern baseline (i.e., modern thermohaline and convective mixing fluxes, surface oxygen concentration, and riverine input). Although our Late Triassic GCM experiments predict thermohaline and convective mixing fluxes, these absolute fluxes are certainly model dependant. In any case, altering the

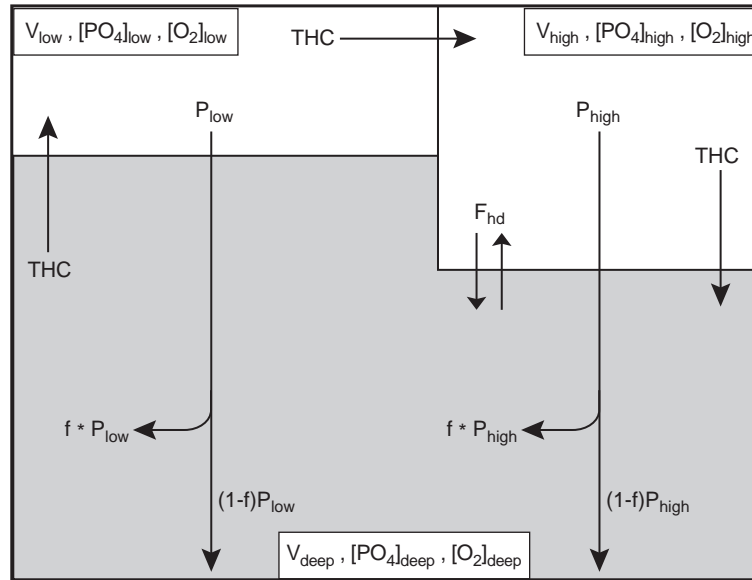


Fig. 8. Schematic of open-system three-box model developed by Hotinski et al. (1999). An open-system box model includes the influences of the riverine input (Riv) organic matter burial. The ocean is divided into three reservoirs: *low* latitude surface ocean, *high* latitude surface ocean, and *deep* ocean. Each reservoir has a corresponding phosphate  $[PO_4]$  and dissolved oxygen  $[O_2]$  concentration, and a characteristic volume  $V$ . The flux of phosphate is transported between reservoirs by the thermohaline circulation (THC), deep convective mixing ( $F_{hd}$ ), and particulate organic matter export ( $P$ ). Most of the particulate organic matter exported to the deep ocean is regenerated according to the regeneration factor ( $f$ ), while a small fraction of the export production is buried  $(1-f)P$ . It is assumed that the low latitude surface ocean phosphate concentration is  $0 \mu\text{mol/L}$  because biological productivity utilizes all nutrients at the surface. High latitude oxygen concentration is also constant through time because it is assumed that the surface ocean is well mixed and equilibrates with the atmosphere. Thus high latitude surface ocean concentration was determined by the surface temperature and salinity (Weiss, 1970). The governing equations used in the box model and the constants are listed in Table 2.

circulation fluxes in the box model changes the response time, but not the equilibrium deep ocean oxygen concentration.

We use the box model simply to show that the oceanographic changes associated with a rise in Late Triassic atmospheric  $CO_2$  plausibly caused biotic stress through substantial lowering of oxygen availability. Because the box model does not have the capability to predict local changes in oxygen availability, we do not assign great significance to the absolute values estimated by the model. The box model's sensitivity to surface oxygen concentration, phosphate delivery from river inflow, thermohaline circulation, and convective mixing at high latitudes are summarized in Fig. 9. Deep ocean oxygen concentration declines with a decrease in surface oxygen concentration, thermohaline circulation, or convective mixing, and an increase in riverine input (Fig. 9). Interestingly, the response time to an increase in riverine input or a decrease in thermohaline circulation is on the

order of several hundred thousand years—similar to the time lag between biotic turnover on land and in the ocean.

Table 2

Equations and parameters used in open-system three-box model developed by Hotinski et al. (1999) model

$$\begin{aligned} (dM_{[PO_4]_{low}}/dt) &= [PO_4]_{deep} THC + Riv - P_{low} = 0 \\ (dM_{[PO_4]_{high}}/dt) &= F_{hd} [PO_4]_{deep} - (F_{hd} + THC) [PO_4]_{high} - P_{high} \\ (dM_{[PO_4]_{deep}}/dt) &= (F_{hd} + THC) [PO_4]_{high} - F_{hd} [PO_4]_{deep} + f(P_{high} + P_{low}) \\ (dM_{[O_2]_{deep}}/dt) &= (F_{hd} + THC) [O_2]_{high} - (F_{hd} + THC) [O_2]_{deep} - fR(P_{high} + P_{low}) \end{aligned}$$

Parameters

$THC = 5.99 \times 10^{20}$ L/ky	$[PO_4]_{deep, initial} = 2.15 \mu\text{mol/L}$
$F_{hd} = 1.51 \times 10^{21}$ L/ky	$[PO_4]_{high, initial} = 1.24 \mu\text{mol/L}$
$P_{high} = 6.5 \times 10^{20}$ $\mu\text{mol/L}$	$[O_2]_{high} = 325 \mu\text{mol/L}$
$Riv = 3.32 \times 10^{19}$ $\mu\text{mol/ky}$	$V_{deep} = 1.37 \times 10^{21}$ L
$R = 169$	$V_{high} = 1.28 \times 10^{19}$ L
$F = 0.983$	

Parameters are appropriate for the modern ocean.

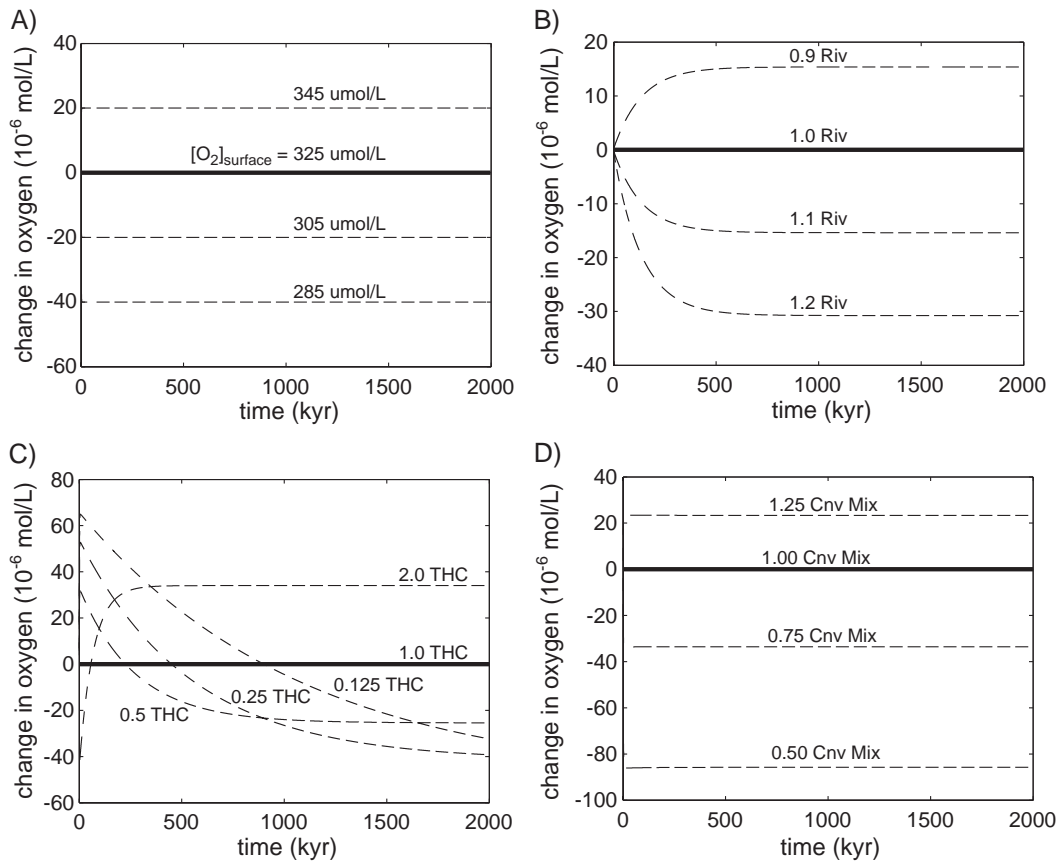


Fig. 9. Box model results under modern-day conditions showing the sensitivity of the deep ocean to changes in (A) high latitude surface oxygen concentration, (B) riverine input of phosphorus, (C) thermohaline circulation, and (D) convective mixing. Changes in oxygen concentrations plotted are mean deep ocean values, in  $10^{-6}$  mol/L. Our Late Triassic model results indicate an increase in riverine input and seawater temperature and decreases in the overturning circulation and convective mixing. These changes are predicted to result in decreases in oxygen availability in the ocean.

In the Late Triassic experiments, the marine response to a rise in atmospheric  $\text{CO}_2$  from 600 to 2400 ppmv include  $>5$  °C surface warming, a 75% reduction in overturning vigor, a  $>50\%$  reduction in convective mixing, and a 10% increase in riverine input. As ocean temperatures rise, oxygen becomes less soluble in seawater (Weiss, 1970). A 5 °C surface warming will reduce the surface oxygen content from 320 to 287  $\mu\text{mol/L}$  (Table 1C), resulting in a 33  $\mu\text{mol/L}$  depletion of oxygen in the deep ocean (Fig. 9A). The box model indicates that a 75% reduction in thermohaline circulation will lead to a 40  $\mu\text{mol/L}$  decline in deep ocean oxygen concentration (Fig. 9C). A 50% decrease in high-latitude convective mixing diminishes deep ocean oxygen concentration by 86  $\mu\text{mol/L}$

(Fig. 9D). Finally, a 10% increase in riverine input (assuming similar river phosphate concentrations) amounts to an additional 15  $\mu\text{mol/L}$  decline of deep ocean oxygen (Fig. 9B). The compounded effects of reduced surface dissolved oxygen concentration, a more sluggish deep circulation, diminished convective mixing, and an increase in river runoff could potentially reduce deep oxygen concentrations by more than 170  $\mu\text{mol/L}$ .

Initializing the three-box model with a surface ocean oxygen concentration of 287  $\mu\text{mol/L}$ , 110% of modern riverine input, and a 4-fold decrease in thermohaline flux, led to deep ocean equilibrium oxygen content of 75  $\mu\text{mol/L}$ . An additional reduction of convective mixing by 25% lowered oxygen

concentrations in the deep ocean to  $<5 \mu\text{mol/L}$ , well within the dysoxic to anoxic range ( $<45 \mu\text{mol/L}$ ) (Arthur and Sageman (1994). Regardless of whether conditions were anoxic, we contend that a sharp decrease in oxygen availability as predicted by the box model would have represented a severe stress on most marine biota.

## 4. Discussion

### 4.1. Linking environmental stress and ecological change

Ecological changes arise from variations in community composition, which are determined by physiological and environmental parameters and the interactions between community members. Environmental conditions affect an organism's physiology (Pörtner, 2002) and determine the nutrient/food supply abundance, as well as habitat space availability (Allmon, 2001). This concept, that species distributions can be defined by climate parameters, is known as the "bioclimate envelope" (cf. Pearson and Dawson, 2003) and has been used to successfully predict species distribution in response to climate change (Pearson et al., 2002). If environmental disturbances are slow and/or small, it can be expected that populations may adapt to the new conditions (Allmon, 2001). However, in areas where environmental stresses are intolerable, populations will either migrate, tracking the geographic position of their bioclimate envelope and invading new territory and causing biogeographic ranges to shift, or go extinct because populations cannot survive or persist. For example, warming of  $\sim 0.6^\circ\text{C}$  over the last century has caused significant poleward and upward shifts in species ranges in a wide range of organisms over very diverse geographical locations (Walther et al., 2002). In any case (adaptation, migration, or extinction), the community composition in a given area is restructured. In the fossil record, these ecological responses will be recorded as biotic turnover, defined as coincident evolutionary appearance and disappearance of species.

Our results indicate that the global mean temperature rises by more than  $6^\circ\text{C}$  with a 4-fold increase in atmospheric  $\text{CO}_2$ . The magnitude of warming

across the T–J boundary simulated here is greater than previous estimates ( $3\text{--}4^\circ\text{C}$ ), which used thermodynamic relationships between  $p\text{CO}_2$  and temperature (e.g., McElwain et al., 1999; Beerling and Berner, 2002). Global average temperature changes an order of magnitude smaller have been shown to have tremendous ecological impact, as noted above. The ecological impact of recent climate change on organisms, populations, and ecological communities has arisen mainly from large regional climate changes and the intensification of climate extremes (Walther et al., 2002; Easterling et al., 2000). The Triassic experiments predict large regional temperature increases ( $>10^\circ\text{C}$  increase in mean annual temperature) and substantial intensification of maximum climate extremes ( $>10^\circ\text{C}$  in maximum daily temperature) with a rise in  $\text{CO}_2$  from  $2\times$  to  $8\times$  pre-industrial levels. Orbital fluctuations would also have influenced climate extremes, at times intensifying them, and potentially promoting further ecological changes. Given the duration of the T–J mass extinction event, the climatic effect of orbital variations must be considered as a possible amplifier of the environmental stresses initially exerted on ecosystems from rising  $\text{CO}_2$ .

In subtropical regions of Pangea, the climate extremes predicted in the Triassic  $8\times$  experiment approach the physiological threshold of modern organisms. For example, metazoans can only temporarily tolerate temperatures greater than  $47^\circ\text{C}$  (cf. Schmidt-Nielsen, 1997), while metazoan populations are unable to withstand temperatures near  $42^\circ\text{C}$  (Pörtner, 2001). The climate thresholds that trigger physiological changes in modern organism are often species-specific (Walther et al., 2002). However, in the case of nonsucculent plants, the threshold temperature for thermal damage to leaves is a highly conservative characteristic among many extant species, occurring at  $\sim 45^\circ\text{C}$  (cf. Schulze and Caldwell, 1994). Measurements of leaf width, stomatal density and size, and  $\delta^{13}\text{C}$  of fossil leaves can be used to calculate leaf temperatures based on energy considerations (cf. McElwain et al., 1999). Employing this methodology, McElwain et al. (1999) estimated that noon leaf temperatures of Late Triassic large leaved plants, such as *Ginkgo*, were at least  $10^\circ\text{C}$  greater than the air temperature. Our sensitivity results suggest that a rise of  $p\text{CO}_2$ , from  $2\times$  to  $8\times$ , will

cause at least a 20-fold expansion in the area where temperatures are fatal to large leaved plants (Table 2; Fig. 2). These results are consistent with the observed extinction of large leaved species at the T–J boundary, and subsequent replacement by species with more dissected leaves, which are more capable of minimizing high temperature injury through increased heat dissipation (McElwain et al., 1999).

In the marine realm, the model predicts a reduction in the overturning circulation and higher ocean temperatures with a rise in atmospheric CO<sub>2</sub>. These stresses in themselves may not have caused marine extinctions. However, according to our simple box model calculations, both of these factors would have led to a substantial decrease in seawater oxygen concentrations. The spread of low-oxygen waters may help explain the collapse in the marine productivity across the T–J boundary (Pálffy et al., 2001; Ward et al., 2001). In addition, rapid (<10<sup>5</sup> years) dissolution of CO<sub>2</sub> in the ocean would have lowered the pH, making the ocean more acidic and less hospitable to marine organisms that secrete calcium carbonate shells and skeletons (Kleypas et al., 1999; Caldeira and Wickett, 2003). In fact, the fossil record indicates that the end-Triassic was marked by an almost complete extermination of coral species and a collapse of the reef ecosystem (Hallam and Goodfellow, 1990).

While the Triassic simulations have demonstrated that increasing atmospheric CO<sub>2</sub> can produce conditions beyond the absolute tolerance of some organisms, it is the change in the environmental parameters—by affecting the size of the bioclimate envelope that will have an effect on most organisms and drive biotic changes. The reshaping of the bioclimate envelope will determine inter-species interactions such as competition, predation, and symbiosis (Pearson and Dawson, 2003) and ultimately affect species distribution. The lack of good understanding of the physiological constraints and responses of Triassic organisms to environmental variables inhibits predictions of precisely how species distributions changed in the past. Nonetheless, the results of these climate simulations predict that Late Triassic organisms may have had to contend with substantial environmental disturbances in the terrestrial and marine realms as a result of rising atmospheric CO<sub>2</sub>.

#### 4.2. Unresolved issues

Most coupled climate models used to simulate future increases of greenhouse gases predict a weakening of the North Atlantic thermohaline circulation due to enhanced regional freshwater forcing (e.g., Manabe and Stouffer, 1993; Kattenberg et al., 1996). Our model results for the Late Triassic demonstrate a similar response to increased atmospheric CO<sub>2</sub>, a reduction in global thermohaline circulation. However, modeling studies have also demonstrated enhanced thermohaline circulation with increased CO<sub>2</sub> forcing for past climates (Otto-Bliesner et al., 2002; Winguth et al., 2002; Vavrus and Kutzbach, 2002). For example, Otto-Bliesner et al. (2002) showed that increasing CO<sub>2</sub> in simulations of the Cretaceous led to destabilization of the upper ocean through enhanced poleward transport of saline waters. The point is that uncertainty still exists regarding the response of meridional overturning to CO<sub>2</sub> forcing.

Under conditions of reduced overturning and convective mixing and higher riverine input as predicted by FOAM with a 4-fold increase in *p*CO<sub>2</sub>, our box model results indicate that the deep ocean may have experienced a severe depletion in oxygen, a result consistent with other modeling studies that have demonstrated oxygen depletion in the water column as a consequence of global warming (Matear and Hirst, 2003) and a reduced equator to pole temperature gradient (Hotinski et al., 2001). However, if the Late Triassic thermohaline circulation was not affected or was enhanced by increasing CO<sub>2</sub>, then our box model would predict an increase in oxygen concentrations (Fig. 9C).

The results of this study have provided a snapshot of possible equilibrium climates before and after the end-Triassic event. This modeling approach gives an estimate of the magnitude of climate change associated with the CO<sub>2</sub> forcing, but reveals nothing about the rate of change. Unfortunately, reliable estimates for the rate of CO<sub>2</sub> increase and environmental change are inhibited by the lack of a precise timescale for many T–J boundary sections (Jenkyns, 2003). Moreover, long (hundreds of thousand of years), transient climate simulations representing the T–J event are not feasible due to the computational expense.

Finally, we view the estimated magnitude of changes predicted in this study as conservative

since the maximum  $p\text{CO}_2$  (2400 ppmv) examined in this study is less than that proposed from paleo-evidence and modeling studies (>2500 ppmv). In addition, the lack of an interactive biome model in FOAM prohibits the land surface from responding to rising  $\text{CO}_2$  and associated climate changes. As a result, the total climate change on land is probably underestimated.

## 5. Summary and conclusions

Coupled ocean–atmosphere GCM experiments indicate that the Late Triassic climate system is highly sensitive to changes in atmospheric  $\text{CO}_2$  concentrations. An end-Triassic rise in atmospheric  $\text{CO}_2$ , postulated to result from volcanic degassing, is predicted to have instigated severe environmental stresses on terrestrial and marine ecosystems. On land, intense continental heat stress, accompanied by very warm continental temperatures, extreme seasonal fluctuations, an intensification of the number of hot and dry days, and an exponential increase in the area affected by heat stress, is predicted. Orbital fluctuations further intensify the environmental stresses exerted on terrestrial ecosystems. In the ocean, increased stratification likely led to a reduction in oxygen availability in the water column.

In closing, model results support the contention that rising  $\text{CO}_2$  in the Late Triassic would have caused severe environmental stress that potentially instigated lagged biological turnover on land and ocean. Although the response of Triassic ecosystems to  $\text{CO}_2$ -driven stresses is unknown, ecosystem models using future climate-warming scenarios (with a much smaller  $\text{CO}_2$ ) predict extinction risks of 15–37% for all species (Thomas et al., 2004). If the ecological response in the Triassic were at all similar to the modern, a severe ecological crisis would be an expected outcome of CAMP volcanic degassing at the end of the Triassic.

## Acknowledgements

We thank F. Surlyk, D. Beerling, and two anonymous reviewers for their constructive comments on this manuscript. We are also grateful to R. Jacob

for technical support of FOAM and D. Bottjer for his encouragement of this project. All climate simulations were performed on the University of Southern California's HPCC Linux Supercomputer.

## References

- Allmon, W.D., 2001. Nutrients, temperature, disturbance, and evolution: a model for the late Cenozoic marine record of the western Atlantic. *Palaeogeography, Palaeoclimatology, Palaeoecology* 166, 9–26.
- Arthur, M.A., Sageman, B.B., 1994. Marine black shales, depositional mechanisms and environments of ancient deposits. *Annual Review of Earth and Planetary Sciences* 22, 499–551.
- Beerling, D.J., Berner, R.A., 2002. Biogeochemical constraints on the Triassic–Jurassic boundary carbon cycle event. *Global Biogeochemical Cycles* 16, 101–113.
- Benton, M.J., 1995. Diversification and extinction in the history of life. *Science* 268, 52–58.
- Berner, R.A., Kothavala, Z., 2001. GEOCARB III: a revised model of atmospheric  $\text{CO}_2$  over Phanerozoic time. *American Journal of Science* 301, 182–204.
- Bice, D.M., Newton, C.R., McCauley, S., Reiners, P.W., McRoberts, C.A., 1992. Shocked quartz at the Triassic–Jurassic boundary in Italy. *Science* 255, 443–446.
- Bown, P.R., Lord, A.R., 1990. The occurrence of calcareous nannofossils in the Triassic–Jurassic boundary interval. *Cahiers de l'Université de Lyon, Série Scientifique* 3, 127–136.
- Caldeira, K., Wickett, M.E., 2003. Anthropogenic carbon and ocean pH. *Nature* 425, 365.
- Cohen, A.S., Coe, A.L., 2002. New geochemical evidence for the onset of volcanism in the Central Atlantic Magmatic Province and environmental change at the Triassic–Jurassic boundary. *Geology* 30, 267–270.
- Colbert, E.H., 1986. Mesozoic tetrapod extinctions: a review. In: Elliot, D.K. (Ed.), *Dynamics of extinctions*. John Wiley and Sons, New York, pp. 49–62.
- Courtillot, V., 1994. Mass extinctions in the last 300 millions years: one impact and seven flood basalts? *Israel Journal of Earth-Sciences* 43, 255–266.
- Crowley, T.J., Baum, S.K., 1992. Milankovitch fluctuations on the supercontinents. *Geophysical Research Letters* 19, 793–796.
- Davis, M.B., Shaw, R.G., 2001. Range shifts and adaptive responses to Quaternary climate change. *Science* 292, 673–679.
- Easterling, D.R., Meehl, G.A., Parmesan, C., et al., 2000. Climate extremes: observations, modeling, and impacts. *Science* 289, 2068–2074.
- Ekart, D.D., Cerling, T.E., Montañez, I.P., Tabor, N.J., 1999. A 400 million year carbon isotope record of pedogenic carbonates: implications for paleoatmospheric carbon dioxide. *American Journal of Science* 299, 805–827.
- El-Shaarawy, Z., 1981. Foraminifera and ostracods of the topmost Triassic and basal Jurassic of England, Wales, and Austria. PhD thesis. University of Birmingham.

- Endel, A.S., Sofia, S., 1981. Rotation in solar-type stars: I. Evolution models from the spin-down of the sun. *Astrophysical Journal* 243, 625–640.
- Fowell, S.J., 1994. Palynology of Triassic–Jurassic boundary sections from the Newark Supergroup of eastern North America: implications for catastrophic extinction scenarios. PhD thesis. Columbia University, New York. 159 p.
- Hallam, A., 1981. The end-Triassic bivalve extinction event. *Palaeogeography, Palaeoclimatology, Palaeoecology* 35, 1–44.
- Hallam, A., Goodfellow, W.D., 1990. Facies and geochemical evidence bearing on the end-Triassic disappearance of the Alpine reef ecosystem. *Historical Biology* 4, 131–138.
- Hallam, A., Wignall, P.B., 1997. Mass extinctions and their aftermath. Oxford University Press, Oxford. 320 p.
- Hames, W.E., Renne, P.R., Ruppel, C., 2000. New evidence for geologically instantaneous emplacement of earliest Jurassic Central Atlantic Magmatic Province basalts on the North American margin. *Geology* 28, 859–862.
- Harrison, S.P., Kutzbach, J.E., Liu, Z.Y., Bartlein, P.J., Otto-Bliesner, B., Muhs, D., Prentice, I.C., Thompson, R.S., 2003. Mid-Holocene climates of the Americas: a dynamical response to changed seasonality. *Climate Dynamics* 20, 663–688.
- Hesselbo, S.P., Robinson, S.A., Surlyk, F., Piasecki, S., 2002. Terrestrial and marine extinction at the Triassic–Jurassic boundary synchronized with major carbon-cycle perturbation: a link to initiation of massive volcanism? *Geology* 30, 251–254.
- Hotinski, R.M., Kump, L.R., Najjar, R.G., 1999. Opening Pandora's Box: the impact of open system modeling on interpretation of anoxia. *Paleoceanography* 15, 267–279.
- Hotinski, R.M., Bice, K.L., Kump, L.R., Najjar, R.G., Arthur, M.A., 2001. Ocean stagnation and the end-Permian anoxia. *Geology* 29, 7–10.
- Huntley, B., 1999. Species distribution and environmental change: considerations from the site to landscape scale. In: Maltby, E., Holdgate, M., Acreman, M., Weir, A. (Eds.), *Ecosystem Management: Questions for Science and Society*. Royal Holloway Institute for Environmental Research, Virginia Water, UK, pp. 115–130.
- Jacob, R.C., 1997. Low frequency variability in a simulated atmosphere ocean system. PhD thesis, University of Wisconsin, Madison, 159 p.
- Jacob, R., Schafer, C., Foster, I., Tobis, M., Anderson, J., 2001. Computational design and performance of the fast ocean atmosphere model, version one. In: Alexandrov, V.N., Dongarra, J.J., Tan, C.J.K. (Eds.), *Proc. 2001 International Conference on Computational Science*. Springer-Verlag, pp. 175–184. Online versions are available at <http://www-unix.mcs.anl.gov/foam/publications.html>.
- Jenkyns, H.C., 2003. Evidence for rapid climate change in the Mesozoic–Palaeogene greenhouse world. *Philosophical Transactions of the Royal Society of London* 361, 1885–1916.
- Kattenberg, A., Giorgi, F., Grassl, H., Meehl, G.A., Mitchell, J.F.B., Stouffer, R.J., Tokioka, A.J.W.T., Wigley, T.M.L., 1996. *Climate change 1995: the science of climate change*. Cambridge University Press, pp. 289–357.
- Kiehl, J.T., Hack, J.J., Bonan, G.B., Boville, B.A., Briegleb, B.P., Williamson, D.L., Rasch, P.J., 1996. Description of the NCAR Community Climate Model (CCM3), NCAR Technical Note NCAR/NT-420+STR, Boulder, CO.
- Kleypas, J.A., Buddemeier, R.W., Archer, D., et al., 1999. Geochemical consequences of increased atmospheric carbon dioxide on coral reefs. *Science* 284, 118–120.
- Liu, Z., Kutzbach, J., Wu, L., 2000. Modeling climate shift of El Niño variability in the Holocene. *Geophysical Research Letters* 27, 2265–2268.
- Liu, Z., Brady, E., Lynch-Stieglitz, J., 2003. Global ocean response to orbital forcing in the Holocene. *Paleoceanography* 18.
- Manabe, S., Stouffer, R.J., 1993. Century-scale effects of increased atmospheric CO<sub>2</sub> on the ocean–atmosphere system. *Nature* 364, 215–218.
- Marzoli, A., Renner, P.R., Piccirillo, E.M., Ernesto, M., Bellieni, G., De Min, A., 1999. Extensive 200-million-year-old continental flood basalts of the Central Atlantic Magmatic Province. *Science* 284, 616–618.
- Matear, R.J., Hirst, A.C., 2003. Long-term changes in dissolved oxygen concentrations in the ocean caused by protracted global warming. *Global Biogeochemical Cycles* 17, 1125.
- Matthews, E., 1983. Global vegetation and land use: new high-resolution databases for climate studies. *Journal of Applied Meteorology* 22, 474–487.
- McElwain, J.C., Beerling, D.J., Woodward, F.I., 1999. Fossil plant and global warming at the Triassic–Jurassic boundary. *Science* 285, 1386–1390.
- McRoberts, C.A., Newton, C.R., 1995. Selective extinction among end-Triassic European bivalves. *Geology* 23, 102–104.
- Moseley, P.L., Gapen, C., Wallen, E.S., Walter, M.E., Peterson, M.W., 1994. Thermal stress induces epithelial permeability. *American Journal of Physiology* 267, C425–C434.
- Olsen, P.E., Shubin, N.H., Anders, M.H., 1987. New Early Jurassic tetrapod assemblages constrain Triassic–Jurassic tetrapod extinction event. *Science* 237, 1025–1029.
- Otto-Bliesner, B.L., Brady, E., Shields, C., 2002. Late Cretaceous Ocean: couple simulations with the NCAR CSM. *Journal of Geophysical Research Atmospheres* 107.
- Pálfy, J., Mortensen, J.K., Carter, E.S., Smith, P.L., Friedman, R.M., Tipper, H.W., 2000. Timing the end-Triassic mass extinction: first on land, then in the sea? *Geology* 28, 39–42.
- Pálfy, J., Demény, A., Haas, M., Hetényi, M., Orchard, M.J., Vető, I., 2001. Carbon isotope anomaly and other geochemical changes at the Triassic–Jurassic boundary. *Geology* 29, 1047–1050.
- Pálfy, J., Smith, P.L., Mortensen, J.K., 2002. Dating the end-Triassic and Early Jurassic mass extinctions, correlative large igneous provinces, and isotopic events. In: Koerber, C., MacLeod, K.G. (Eds.), *Catastrophic events and mass extinctions: impacts and beyond*, Special Paper-Geological Society of America, vol. 356. Geological Society of America, Boulder, CO, pp. 523–532.
- Pearson, R.G., Dawson, T.P., 2003. Predicting the impacts of climate change on the distribution of species: are bioclimate envelope models useful? *Global Ecology and Biogeography* 12, 361–371.

- Pearson, R.G., Dawson, T.P., Berry, P.M., Harrison, P.A., 2002. SPECIES: a spatial evaluation of climate impact on the envelope of species. *Ecological Modelling* 154, 289–300.
- Pierrehumbert, R.T., 2004. High levels of atmospheric carbon dioxide necessary for the termination of global glaciation. *Nature* 429, 646–649.
- Pörtner, H.O., 2001. Climate change and temperature dependent biogeography: oxygen limitation of thermal tolerance in animals. *Naturwissenschaften* 88, 137–146.
- Pörtner, H.O., 2002. Climate variations and the physiological basis of temperature dependent biogeography: systematic to molecular hierarchy of thermal tolerance in animals. *Comparative Biochemistry and Physiology. Part A* 132, 739–761.
- Poulsen, C.J., 2001. Impact of ocean dynamics on the simulation of the Neoproterozoic “snowball Earth”. *Geophysical Research Letters* 28, 1575–1578.
- Poulsen, C.J., Gendaszek, A.S., Jacob, R.L., 2003. Did the rifting of the Atlantic Ocean cause the Cretaceous thermal maximum? *Geology* 31, 115–118.
- Raup, D.M., Sepkoski Jr., J.J., 1982. Mass extinction in marine fossil record. *Science* 215, 1501–1503.
- Retallack, G.J., 2002. Triassic–Jurassic atmospheric CO<sub>2</sub> spike. *Nature* 296, 1812–1813.
- Rifkind, J.M., Abugo, O., Levy, A., Monticone, R., Heim, J., 1993. Formation of free radicals under hypoxia. In: Hochachka, P.W., Lutz, P.L., Sick, T., Rosenthal, M., van den Thillart, G. (Eds.), *Surviving Hypoxia: Mechanisms of Control and Adaptation*. CRC Press, Boca Raton, FL, pp. 509–525.
- Royer, D.L., Berner, R.A., Beerling, D.J., 2001. Phanerozoic atmospheric CO<sub>2</sub> change: evaluating geochemical and paleobiological approaches. *Earth-Science Reviews* 54, 349–392.
- Schmidt-Nielsen, K., 1997. *Animal physiology: adaptation and environment*, 5th edition. Cambridge University Press, Cambridge. 607 p.
- Schulze, E.D., Caldwell, M.M., 1994. *Ecophysiology of photosynthesis*. Springer-Verlag, Berlin. 576 p.
- Scotese, C.R., Worsley, T.R., Moore, T.L., Fraticelli, C.M., 1994. Phanerozoic CO<sub>2</sub> levels and global temperatures inferred from changing paleogeography. In: Klein, G.D. (Ed.), *Pangea: Paleoclimate, Tectonics, and Sedimentation During Accretion, Zenith, and Breakup of a Supercontinent*, Special Paper Geological Society of America vol. 288. Geological Society of America, Boulder, CO, pp. 57–73.
- Sepkoski Jr., J.J., 1996. Patterns of Phanerozoic extinction: a perspective from global databases. In: Walliser, O.H. (Ed.), *Global Events and Event Stratigraphy*. Springer-Verlag, New York, pp. 35–51.
- Stothers, R.B., 1993. Flood basalts and extinction events. *Geophysical Research Letters* 20, 1399–1402.
- Suchocki, R.K., Hubert, J.F., Birney de Wit, C.C., 1988. Isotopic imprint of climate and hydrogeochemistry on terrestrial strata of the Triassic–Jurassic Hartford and Fundy rift basins. *Journal of Sedimentary Petrology* 58, 801–811.
- Tanner, L.H., Hubert, J.F., Coffey, B.P., 2001. Stability of atmospheric CO<sub>2</sub> across the Triassic–Jurassic boundary. *Nature* 411, 675–677.
- Thomas, C.D., Cameron, A., Green, R.E., et al., 2004. Extinction risk from climate change. *Nature* 427, 145–148.
- Vavrus, S., Kutzbach, J.E., 2002. Sensitivity of the thermohaline circulation to increased CO<sub>2</sub> and lowered topography. *Geophysical Research Letters* 29.
- Visscher, H., Brugman, W.A., 1981. Ranges of selected palynomorphs in the Alpine Triassic of Europe. *Review of Palaeobotany and Palynology* 34, 115–128.
- Walther, G., Post, E., Convey, P., et al., 2002. Ecological responses to recent climate change. *Nature* 416, 389–395.
- Ward, P.D., Haggart, J.W., Carter, E.S., Wilbur, D., Tipper, H.W., Evans, T., 2001. Sudden productivity collapse associated with the Triassic–Jurassic boundary mass extinction. *Science* 292, 1148–1151.
- Weiss, R.F., 1970. The solubility of nitrogen, oxygen, and argon in water and seawater. *Deep Sea Research* 17, 721–725.
- Winguth, A.M.E., Heinze, C., Kutzbach, J.E., Maier-Reimer, E., Mikolajewicz, U., Rowley, D., Rees, A., Ziegler, A.M., 2002. Simulated warm polar currents during the middle Permian. *Paleoceanography* 17.
- Woodward, F.I., 1987. *Climate and plant distribution*. Cambridge University Press, Cambridge.
- Wu, L.X., Liu, Z.Y., 2002. Is tropical Atlantic variability driven by the North Atlantic oscillation? *Geophysical Research Letters* 29.
- Yapp, C.J., Poets, H., 1996. Carbon isotopes in continental weathering environments and variations in ancient atmospheric CO<sub>2</sub> pressure. *Earth and Planetary Science Letters* 137, 71–82.